Chemical Engineering Journal 295 (2016) 1–10

Contents lists available at ScienceDirect

Chemical Engineering Journal

journal homepage: www.elsevier.com/locate/cej

CO_2 reforming of CH_4 over Ni–Co/MSN for syngas production: Role of Co as a binder and optimization using RSM

S.M. Sidik [a], S. Triwahyono [b,*], A.A. Jalil [a,c], Z.A. Majid [b], N. Salamun [b], N.B. Talib [b], T.A.T. Abdullah [a,c]

[a] Department of Chemical Engineering, Faculty of Chemical and Energy Engineering, Universiti Teknologi Malaysia, 81310 UTM Johor Bahru, Johor, Malaysia
[b] Department of Chemistry, Faculty of Science, Universiti Teknologi Malaysia, 81310 UTM Johor Bahru, Johor, Malaysia
[c] Centre of Hydrogen Energy, Institute of Future Energy, Universiti Teknologi Malaysia, 81310 UTM Johor Bahru, Johor, Malaysia

HIGHLIGHTS

- The Co binder was added into Ni/MSN catalyst using consecutive in situ electrolysis.
- At similar metal content, the Ni–Co/MSN gave a higher activity compared to Ni/MSN.
- The formation of Ni–Co alloy reduced sintering and coke formation in the catalyst.
- The ANOVA analysis showed that temperature is the most significant variable in RSM.
- The optimum CH_4 conversion reached 97% at 768 °C and GHSV of 38,726 mL g^{-1} h^{-1}.

GRAPHICAL ABSTRACT

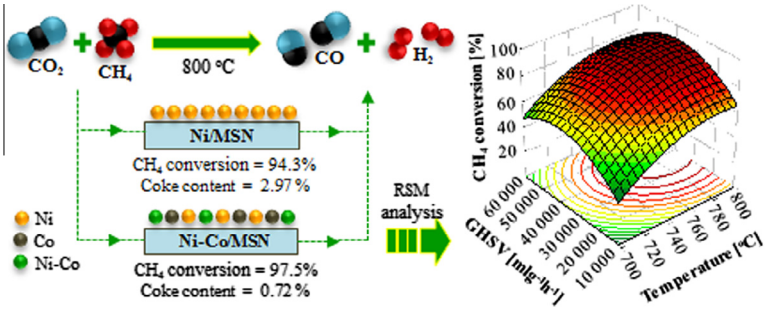

ARTICLE INFO

Article history:
Received 20 December 2015
Received in revised form 26 February 2016
Accepted 8 March 2016
Available online 12 March 2016

Keywords:
Nickel
Cobalt
Bimetallic
CO_2 reforming of CH_4
Optimization

ABSTRACT

A bimetallic Ni–Co catalyst supported on MSN (Ni–Co/MSN) was prepared by consecutive in situ electrolysis method. XRD and XPS results revealed that the addition of Co as a binder induced the formation of $NiCo_2O_4$, a spinel-type solid solution. The results implied a *d*-electron transfer from Co to Ni, which increased the electron density of Ni in the Ni–Co/MSN. The formation of Ni–Co alloy in the Ni–Co/MSN helped in decreasing the Ni particle size, providing better metal dispersion, and established a stronger interaction between Ni and Co, as evidenced by TEM and H_2-TPR analyses. In comparison to the Ni/MSN, the Ni–Co/MSN exhibited higher activity up to 97.5% CH_4 conversion and stability for more than 30 h time on stream. The high performance of the Ni–Co/MSN was due to the synergistic effect between Ni and Co, small Ni particle size and better Ni dispersion. The enrichment of electron on Ni particles and high anti-sintering ability of the Ni–Co/MSN catalyst were responsible to maintain the stability of the catalyst. The analysis of variance (ANOVA) analysis indicated that reaction temperature was the prominent significant single variable that affected the CH_4 conversion, followed by interaction of temperature and CO_2/CH_4 ratio and quadratic interaction of GHSV. The optimum CH_4 conversion predicted from the response surface analysis is 97% at reaction temperature of 783 °C, CO_2:CH_4 ratio of 3, and GHSV of 38,726 mL g^{-1} h^{-1}.

1. Introduction

In recent years, the CO_2 reforming of CH_4 has shown an increasing interest for syngas production and as chemical energy transmission system. This process produces unity ratio of syngas, which can be

* Corresponding author. Tel.: +60 7 5536076; fax: +60 7 5536080.
E-mail address: sugeng@utm.my (S. Triwahyono).

http://dx.doi.org/10.1016/j.cej.2016.03.041
1385-8947/

preferentially used for the production of Fischer–Tropsch liquid hydrocarbon and oxygenates. The most important advantage to be offered by CO_2 reforming of CH_4 is the utilization of harmful greenhouse gases (CO_2 and CH_4). This process will be a potential process for the production of syngas in the future along with steam reforming and partial oxidation of reforming process. However, commercialization of CO_2 reforming of CH_4 technology remains a great challenge as it suffers from severe catalyst deactivation through coke deposition and metal sintering. Because of its endothermic character, the CO_2 reforming of CH_4 requires a high reaction temperature. Thermodynamic data indicate that this reaction is not spontaneous at atmospheric pressure below 906 K [1] and, that side reactions, mainly CH_4 decomposition to produce coke, take place at a significant rate between 906 K and 973 K. This means that the reaction must be carried out at reaction temperature higher than 973 K.

Metals of groups 8, 9, and 10 (except osmium) are able to catalyze CO_2 reforming of CH_4 [2]. The noble metals such as Rh, Ru and Pt are expensive and of limited availability, so, in practice, they are not suitable for this process at industrial level. In spite of that rapid deactivation owing to carbon deposition and/or sintering of active metals at high temperatures is always observed, Ni-based catalysts have attracted considerable interest for their low costs and high activities. It has been proved that the presence of modifiers [3] can inhibit the coke formation and extend the lifetime of the catalyst. One of the most important options for enhancing activity and stability in CO_2 reforming of CH_4 is to use bimetallic catalysts.

Bimetallic catalyst system with respect to active surface elements can provide few advantages for CO_2 reforming of CH_4. Liu et al. [4] studied a series of catalyst modifiers including Ti, Mn and Zr incorporated into Ni-based catalysts and found that Ni–Zr bimetallic catalyst exhibited higher activity and better stability compared to the other two catalysts. It was attributed to strong anchoring effects of Zr^{4+} and partial activation of CO_2 by Zr^{4+}. Besides those mentioned modifiers, Co has attracted recent interest as the second metal to be doped with Ni to form bimetallic catalysts. The high activity of Co-based catalysts is related to its ability in methane decomposition reaction [5]. Fan et al. reported that the catalytic performance of monometallic Ni and Co catalysts was improved through synergized effect of both components in bimetallic catalysts which showed better activity and regenerability [6]. Similar bimetallic catalyst system reported by Zhang et al. exhibited great tolerance to coke formation due to the synergistic effects, highly dispersed active metal and strong metal-support interactions [1].

In recent years, mesoporous silica nanoparticles (MSN) have been well developed as effective materials in the field of adsorption [7], drug delivery [8] and catalysis [9,10]. Their high surface area (900–1100 $m^2\,g^{-1}$) and the presence of uniform pore sized lined with silanol groups is helpful to disperse active metal particles and provide mild basicity, which is required in CO_2 reforming of CH_4. In this work, bimetallic Ni–Co supported on MSN (Ni–Co/MSN) was prepared using a consecutive in situ electrochemical method. As previous investigation has shown [10,11], the smaller particle size of the electrogenerated metal particles enhanced specific surface area and active sites available for the reaction. The aims of this study are as follows: (i) preparing Ni–Co/MSN as a bimetallic catalyst, (ii) evaluation of the effect of the bimetallic catalyst on the physicochemical properties of the catalysts and (iii) optimization of the activity of the catalysts in CO_2 reforming of CH_4 by response surface methodology (RSM).

2. Experimental

2.1. Synthesis of mesoporous silica nanoparticles (MSN)

MSN was prepared by co-condensation and sol-gel method as previously reported [7]. In brief, the cetyltrimethylammonium bromide (CTAB, Merck), ethylene glycol (EG, Merck) and ammonium (NH_4OH, QRec) solution were dissolved in 700 mL of double distilled water with the following mole composition of CTAB:EG:NH_4-OH:H_2O = 0.0032:0.2:0.2:0.1. After vigorous stirring for about 30 min at 50 °C, 1.2 mmol tetraethylorthosilicate (TEOS, Merck) and 1 mmol 3-aminopropyl triethoxysilane (APTES, Merck) were added to the clear mixture to give a white suspension solution. This solution was then stirred for another 2 h at 80 °C, and the as-synthesized MSN was collected by centrifugation at 20,000 rpm. The as-synthesized MSN was dried at 110 °C and calcined at 550 °C for 3 h to form surfactant-free MSN. Complete removal of the surfactant was verified by means of infrared spectroscopy, which did not reveal the presence of any residual organic species.

2.2. Preparation of Ni–Co supported on MSN (Ni–Co/MSN)

In this study, the Ni–Co/MSN was prepared by consecutive in situ electrochemical method. Firstly, 2.5 wt.% of Co/MSN catalyst was prepared by adding 10 mL of DMF solution to a one-compartment glass cell fitted with a platinum (Pt) plate cathode (2 cm × 2 cm) and a cobalt (Co) plate anode (2 cm × 2 cm) containing TEAP, naphthalene and MSN. Naphthalene was used as a mediator in the system to produce radical anions, which then reduced the nickel cations to give smaller nickel nanoparticles [12]. Then, the electrolysis was conducted at a constant current of 480 mA cm^{-2} and 0 °C under a N_2 atmosphere under continuous stirring. The time required for complete electrolysis of desired Co loading was calculated based on the Faraday's law, as shown in the following equation;

$$n = \left(\frac{It}{F}\right)\left(\frac{1}{z}\right) \quad (1)$$

where n is the number of moles of Co, I is the constant current of electrolysis (A), t is the total time the constant current was applied (s), F is Faraday's law constant (96,487 C mol^{-1}), and z is the valence number of ion of the substance (electron transferred per ion). For example, 569 s is the time required to produce 2.5 wt.% of Co in 1.5 g MSN. After electrolysis, the solvent was removed before being dried overnight at 110 °C and calcined for 3 h at 550 °C to give a dark blue colored Co/MSN. After that, consecutive addition of 2.5 wt.% of Ni was added to the Co/MSN using the same in situ electrochemical procedures to produce Ni–Co/MSN. As a reference, 5 wt.% of the monometallic Co/MSN and Ni/MSN were also prepared.

2.3. Characterization

The crystalline structure of the catalysts was determined with X-ray diffraction (XRD) recorded on powder diffractometer (Bruker Advance D8, 40 kV, 40 mA) using a Cu Kα radiation source in the range of 2θ = 1.5–80°. The crystallite size of NiO (d_{NiO}) was calculated by means of the Scherrer equation:

$$d_{NiO} = \frac{0.9\lambda}{B\cos\theta} \quad (2)$$

where λ is the X-ray wavelength corresponding to Cu Kα radiation (0.15406 nm), B is the broadening (in radians) of the Ni (200) reflection and θ is the angle of diffraction corresponding to the peak broadening. Nitrogen adsorption–desorption isotherms were used to determine the textural properties at liquid nitrogen temperatures using a Beckman Coulter SA 3100 Surface Area Analyzer. Prior to measurement, all of the catalysts were outgassed at 110 °C for 3 h before being subjected to N_2 adsorption at −196 °C. The morphology of the catalysts as well as semi-quantitative determination of percentage metal loaded were observed by field emission scanning

electron microscopy coupled with energy dispersive X-ray spectrometer (FESEM–EDX) (JSM-6710 F). Transmission electron microscopy (TEM) was carried out using a JEOL JEM-2100F microscope. The samples were ultrasonically dispersed in acetone and deposited on an amorphous, porous carbon grid. H_2-TPR experiments were carried out using Micromeritics Chemisorb 2720 Pulse Chemisorption in 10% H_2/Ar at 10 °C min^{-1}. H_2 chemisorption was measured to investigate the Ni dispersion and Ni surface area of the catalysts. Prior to the chemisorption, 30 mg of the catalyst was reduced with pure H_2 (20 mL min^{-1}) at 900 °C for 1 h. Fourier Transform Infrared (FTIR) measurements were carried out using Agilent Technologies Cary 640 FTIR Spectrometer. To identify the chemical functional groups present in the catalysts, the catalysts was finely ground and dispersed into KBr powder-pressed pellets with a ratio of 1 mg catalyst/100 mg KBr. X-ray photoelectron spectroscopy (XPS) was used for surface analysis and metal oxidation state investigation using an Shimadzu Axis Ultra DLD spectrometer, using Al X-ray source. The charging effect was corrected by adjusting the C 1s peak to a position of 284.5 eV. The sample was pressed into disc and mounted on a sample rod in a pretreatment chamber. The spectra of Ni 2p and Co 2p were recorded and deconvoluted using Casa XPS software.

2.4. Catalytic testing

The catalytic CO_2 reforming of CH_4 was performed in a fixed-bed continuous flow reactor at 300–800 °C. Prior to the reaction, 0.2 g of the catalyst was charged into an ID 4 mm quartz tube, and then it was subjected to O_2 treatment (O_2 = 50 mL min^{-1}) at 850 °C for 1 h, followed by H_2 reduction (H_2 = 50 mL min^{-1}) at 850 °C for 3 h. Then, the reactor was cooling down to a reaction temperature under N_2 stream. CO_2 and CH_4 were mixed at a stoichiometric ratio of 1:1 and N_2 was added as the carrier gas. The reactants with space velocity around 15, 000 mL g^{-1} h^{-1} was passed over the activated catalyst and the products were analyzed using online 6090N Agilent Gas Chromatograph equipped with Carboxen 1010 packed column and TCD detector. The CH_4 conversion was calculated according to the following terms:

$$X_{CH_4} = \frac{[CH_4]_{in} - [CH_4]_{out}}{[CH_4]_{in}} \times 100 \quad (3)$$

where $[CH_4]_{in}$ and $[CH_4]_{out}$ are the molar concentration of CH_4 in the feed and effluent, respectively.

2.5. Experimental design and optimization

In this study, design of experiment (DOE) was used to study the effect of important process variables in the CO_2 reforming of CH_4. Response surface methodology (RSM), a combination of statistical and mathematical technique was used to obtain the optimum value of the process variables [13]. The main objective of RSM is to find an appropriate model for predicting and optimizing the responses. The optimum value of independent variables is determined by finding a point (maximum or minimum point) known as stationary point [14]. A standard RSM analysis coupled with central composite design (CCD) used to generate reasonable experimental runs as well as to analyze the interaction between the variables. The quadratic equation model is employed as represented by the equation below:

$$y = \beta_o + \sum_{i=1}^{k}\beta_i + \sum_{i=1}^{k}\beta_{ii}x_i^2 + \sum\sum_{i=1}^{k}\beta_{ij}x_i x_j + \varepsilon \quad (4)$$

where y is the calculated response, β_o is the intercept term, β_i, β_{ij} and β_{ii} are the measure of the effect of variable x_i, $x_i x_j$, and x_i^2, respectively. The analysis of variance (ANOVA) for the generated regression model was also carried out to ensure its statistical significance. The CCD suggested 2^n factorial runs, 2^n axial runs and n center runs (two replicates), with n as number of factors. The axial point was collected at (±α, 0, 0), (0, ±α, 0), and (0, 0, ±α) where α is the distance of the axial point from center to make the design rotatable. Value of α for CCD was fixed at 1 for the present study. Three process variables selected in this study are reaction temperature (700–800 °C), CH_4 to CO_2 ratio (5–1) and gas hourly space velocity, GHSV (20, 000–60, 000 mL g^{-1} h^{-1}). The range and coded level of the process variables are listed in Table S1. These ranges were predicted based on the results of previous studies [15–17] and preliminary works that have been conducted. A total of 16 experiments were required accordingly to the CCD design. The sequence of experiment was randomized in order to minimize the effect of the uncontrolled factor. The response was monitored as a function of CH_4 conversion. Then, the results were analyzed using a regression analysis program coupled with ANOVA analysis at 10% significance level incorporated in Statsoft Statistica 8.0 software.

3. Results and discussion

3.1. Effect of the addition of Co binder on Ni/MSN catalyst

3.1.1. XRD analysis

Fig. 1 shows the XRD patterns for MSN, NiO, Co_3O_4, Ni/MSN, Co/MSN and Ni–Co/MSN. Low-angle XRD pattern (Fig. 1A) of MSN, Ni/MSN, Co/MSN and Ni–Co/MSN exhibited three distinct peaks at 2θ = 2.35, 4.05 and 4.75°, which can be assigned to (100), (110), and (200) reflections of a hexagonal mesoporous structure (*p6mm*) of the MSN [8]. The intensity of these peaks slightly decreased for Ni/MSN and Co/MSN, indicating a slight distortion of the ordered mesoporous structure after the modification. However, a significant decrease in intensity was observed for Ni–Co/MSN, demonstrating a greater distortion of the structure. Since the MSN is not crystalline at the atomic and molecule levels, no reflection was observed at higher angles. As shown in Fig. 1B, the NiO, Ni/MSN and Ni–Co/MSN exhibited four diffraction peaks at 2θ = 37.3, 43.2, 63.1, and 75.6°, corresponding to (111), (200),

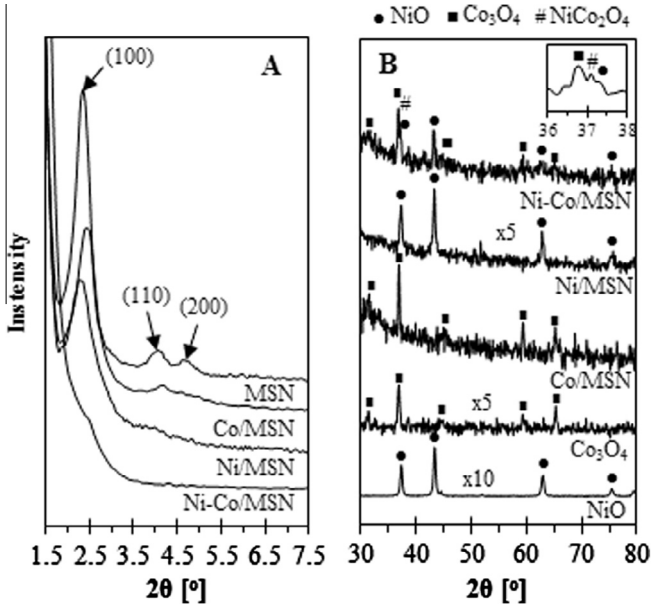

Fig. 1. (A) Low and (B) wide angle of XRD patterns for MSN, Co/MSN, Ni/MSN, Ni–Co/MSN, Co_3O_4 and NiO.

(220), and (311) planes of NiO, respectively (JCPDS 78-0643). The Co_3O_4, Co/MSN and Ni–Co/MSN exhibited five peaks at $2\theta = 31.6$, 36.8, 44.7, 59.6, and 75.6°, corresponding to (220), (311), (400), (422), and (620) planes of Co_3O_4, respectively (JCPDS 42-1467). Besides, there is a new diffraction peak at $2\theta = 37.1°$ was observed in the XRD pattern of Ni–Co/MSN, attributed to the characteristic peak of $NiCo_2O_4$ phase (JCPDS 73-1702). It appears that the simultaneous presence of Ni and Co oxide facilitates the formation of Ni–Co alloy [18]. Sengupta et al. reported that partial dissolution of the Ni oxide phase may possibly occur during the presence of Co oxide due to the similar lattice parameter of these metals [19]. The crystal size of NiO in the Ni/MSN and Ni–Co/MSN calculated using the Scherer equation is 5.62 and 3.87 nm, respectively.

3.1.2. Morphology and particle size

Fig. 2 shows FESEM and TEM images of the MSN, Co/MSN and Ni–Co/MSN. The FESEM image of MSN (Fig. 2A) demonstrated the formation of uniform spherical particles in the size of 40–60 nm. The Co/MSN catalyst retained the spherical morphology (Fig. 2B), with an increase in the surface roughness of catalyst, which is due to the deposition of Co crystallites. Consecutive addition of Ni in the Co/MSN catalyst showed the existence of new pyramidal particles in the Ni–Co/MSN (Fig. 2C). Further EDX-mapping analysis of the pyramidal particles (Fig. S1) elucidated the main composition of this structure is Ni and Co, which suggested that the Ni and Co particles are located closed to each other and possibly might formed an interaction. In the TEM image, MSN showed clusters of hexagonally-ordered silica nanoparticles overlapping each other and formed honeycomb-like structures (Fig. 2D). The ordering of the hexagonal silica decreased after the incorporation of Co and Ni–Co, since no clear long-range silica arrangement was found in those catalysts (Fig. 2E and F, respectively). This may be due to the desilication and structural rearrangement of the silica during the in situ electrochemical incorporation of the Co and/or Ni [20]. This observation is in agreement with the XRD results (Fig. 1A), which revealed that incorporation of the Co and/or Ni led to distortion in the hexagonal silica order. Insert Fig. 2E and F shows the particle size distribution of the metal particles in the Co/MSN and Ni–Co/MSN. The Ni–Co/MSN presented a more homogeneous and smaller average particle size about 3.84 nm compared to the Co/MSN that has an average particle size of 5.68 nm. The smaller particle size of Ni in the Ni–Co/MSN catalyst is might due to the confinement of Ni particle in the Ni–Co solid solution. In fact, it was observed that the distribution of metal was more dispersed in the Ni–Co/MSN compared to the Co/MSN, which might serves a greater number of accessible active metal sites in the CO_2 reforming of CH_4. The small metal particle and better metal dispersion will contribute to more edges and more metal-support structures [1], and leading to more active sites for the reaction to take place. Whereas, the bigger metal particle tend to agglomerate with each other, thus limiting the number of active site for the reactants accessibility.

3.1.3. N_2 adsorption–desorption analysis

The textural properties of the MSN, Co/MSN and Ni–Co/MSN were determined by N_2 adsorption–desorption analysis. The N_2 adsorption–desorption isotherms and pore size distributions of the catalysts are illustrated in Fig. 3. According to the IUPAC classification, the isotherm of the catalysts exhibited typical Type IV adsorption steps at $P/P_o = 0$–0.1, 0.3–0.4, and 0.9–1.0, which could be classified as a mesoporous material. Although the adsorption steps clearly remained for Co/MSN and Ni–Co/MSN, these catalysts showed a remarkable decrease in N_2 adsorption and pore volume compared to the MSN. This indicated that the rearrangement of silica order and pore fillings were occurred during the metal incorporation. In the pore size distributions, all the catalysts demonstrated a bimodal pore structure in the range of 3–20 nm and 20–80 nm. Compared to the MSN, the intensity of pore distribution in both ranges decreased with the addition of Co or/and Ni. This observation is correlated with the reduction in the quantity of adsorbed N_2 in Co/MSN and Ni–Co/MSN at $P/P_o = 0$–0.05 and 0.9–1.0, which indicates the reduction of micropores and interparticles void mesopores. In this study, MSN showed the highest surface area and pore volume about 894 $m^2\,g^{-1}$ and 0.979 $cm^3\,g^{-1}$, respectively. The addition of Co or/and Ni to the MSN resulted in reduction of the surface area and pore volume to 509 and 316 $m^2\,g^{-1}$,

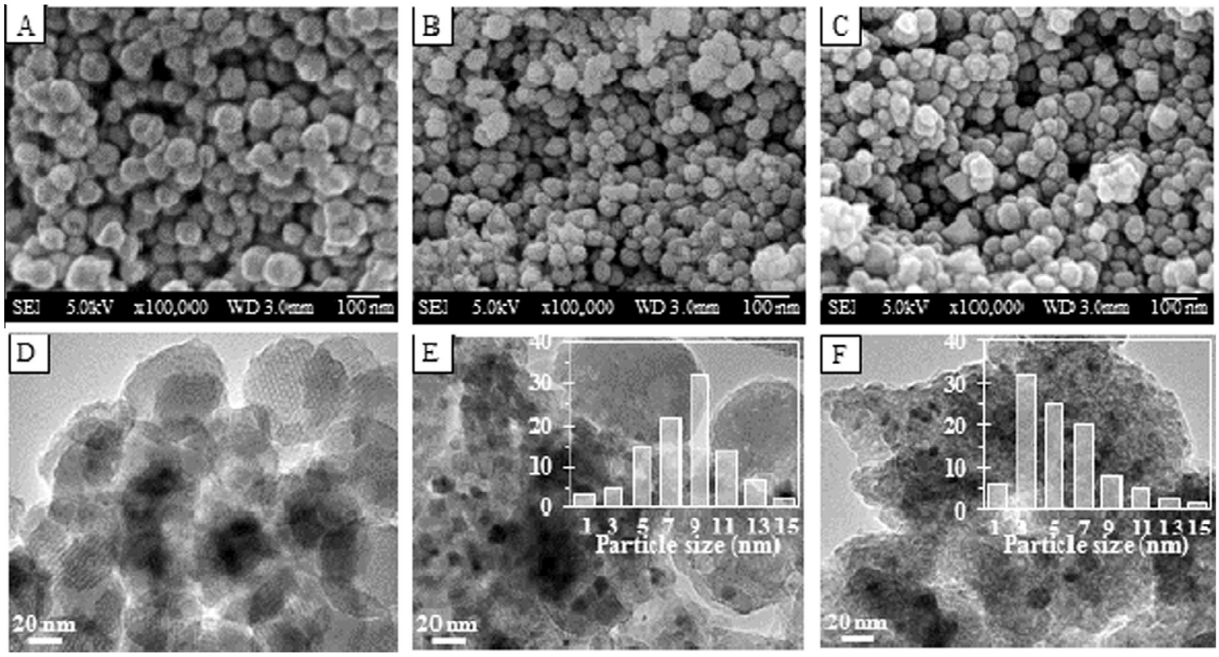

Fig. 2. (A–C) FESEM images of MSN, Co/MSN and Ni–Co/MSN. (D–F) TEM images of MSN, Co/MSN and Ni–Co/MSN. Insert figure (E) and (F) are the HR-TEM particle size distributions of Co/MSN and Ni–Co/MSN.

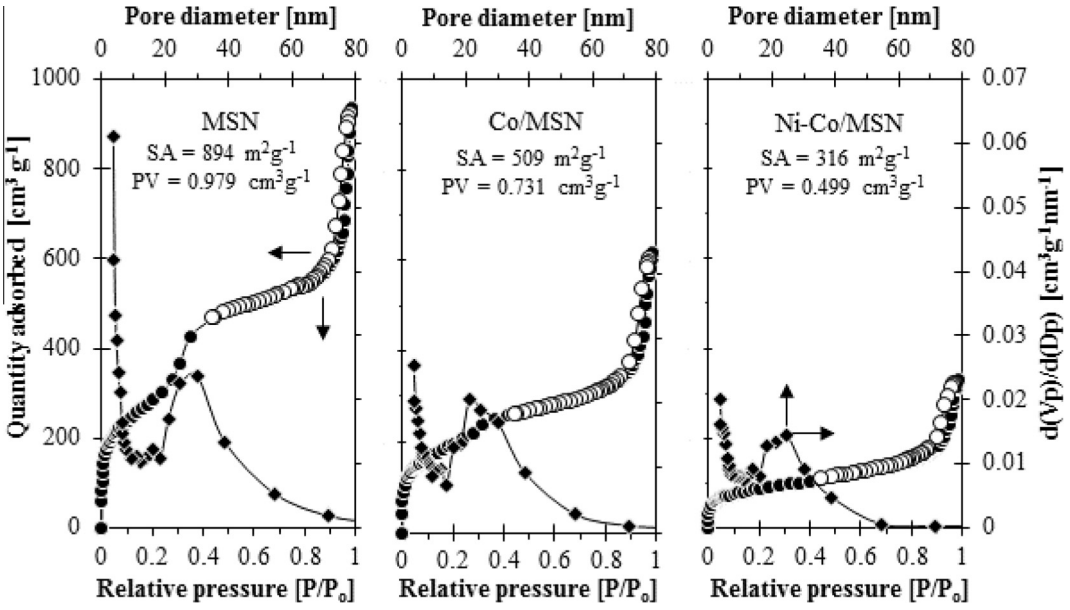

Fig. 3. N_2 adsorption–desorption isotherms and pore size distribution of MSN, Co/MSN and Ni–Co/MSN.

and 0.731 and 0.499 $cm^3\ g^{-1}$, respectively. A decrease in surface area and pore volume with the addition of Co and Ni–Co was attributed to partial pore blockage and/or pore filling of the catalysts.

3.1.4. Reducibility study

TPR technique is used not only to characterize metal-support interactions but also to elucidate the role of additives as binders in the reduction and the influence of one or more phases on the reducibility of a specific compound in multi-component system. In our previous works [10,11], H_2-TPR had been employed to measure the reducibility of Ni/MSN. The broad H_2 consumption area of the Ni/MSN started at 320 °C and continued to about 500 °C. The broad peak area apparently consisting of several overlapping reduction peaks and was deconvoluted into three peaks at 378, 410 and 491 °C, corresponding to the small Ni_2O_3, small NiO and highly dispersed Ni^{2+} that strongly interacted with the MSN. In Fig. 4, the TPR profile of pure Co_3O_4 exhibited two broad peak centered at 382 and 465 °C, which can be assigned to the stepwise reduction of Co_3O_4 to metallic Co. The reduction peak at 382 °C apparently attributed to the reduction of Co_3O_4 (Co^{3+}) to CoO (Co^{2+}), and the higher reduction temperature at 465 °C was needed to reduce CoO to Co^0 [21]. In situ incorporation of the Co into MSN presented different reduction profiles with the pure Co_3O_4, due to the emergence of a sharp peak at 559 °C. By analogy to previous study, the new peak observed at higher temperature can be attributed to the reduction of Co that strongly interacted with MSN support. Thus it can be inferred that very strong interactions exist between Co and MSN support compared to the Ni and MSN. The addition of Co binder to the Ni/MSN catalyst shifted the original reduction profiles of the Ni/MSN to a comparatively higher temperature. The formation of Ni–Co alloy is reflected by reduction at considerably higher temperature due to stronger interaction between the two metals [22]. This result suggested that the addition of Co binder in the Ni/MSN promotes a higher reducibility and stronger interaction, which could enhance the sintering resistant ability of the catalyst [18].

3.1.5. Spectroscopic study

Fig. 5 shows the FTIR results of all catalysts in the range of 400–1600 cm^{-1}. For MSN, three absorption peaks were observed

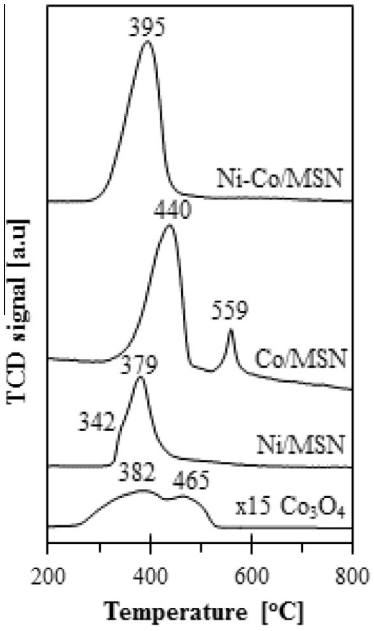

Fig. 4. H_2-TPR profiles of Co_3O_4, Ni/MSN, Co/MSN and Ni–Co/MSN.

at 1091, 790, and 460 cm^{-1} attributed to asymmetric stretching, bending vibration, and symmetric stretching of framework Si–O–Si, respectively [7]. The peak at 956 cm^{-1} is assigned to Si–OH stretching vibration of non-bridging oxygen [8]. Upon the introduction of Co into MSN, the intensity of these peaks decreased which suggesting partial replacement of the Si–O–Si and Si–OH with Co–O–Si. Besides, two sharp peaks at 576 and 666 cm^{-1} corresponding to Co–O vibrations appeared in the Co/MSN spectrum, indicated a successful incorporation of the Co in the catalyst. Further addition of Ni to the Co/MSN resulted in the disappearance of the Co–O vibration bands. This is probably due to the interaction between Ni and Co species in the Ni–Co/MSN. Previous study dealing with the interaction of NiO and Co_3O_4 suggested a strong possibility of the formation of Ni–Co alloy in a bimetallic system due to the closeness of lattice parameter [18].

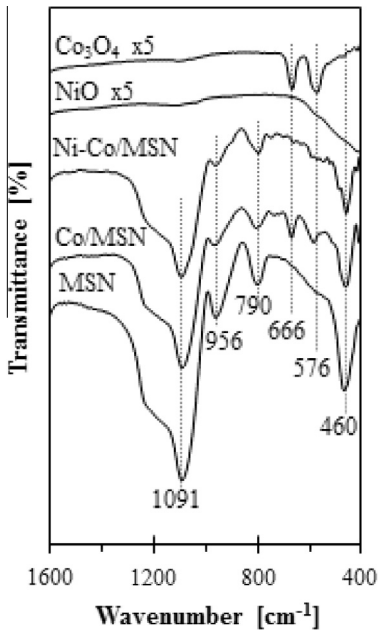

Fig. 5. IR-KBr spectra of MSN, Co/MSN, Ni–Co/MSN, NiO and Co_3O_4.

XPS analysis was carried out to obtain more insight into the surface composition and the oxidative state of metal in the catalysts. Fig. 6 shows the Ni 2p and Co 2p spectra of Ni/MSN, Co/MSN and Ni–Co/MSN. The Ni 2p spectra of Ni/MSN showed Ni $2p_{3/2}$ and Ni $2p_{1/2}$ peaks at 854.2 and 871.2 eV, respectively and the corresponding satellite peaks are observed at 859.2 and 877.9 eV, respectively [23]. In the case of Ni–Co/MSN, the peak of Ni $2p_{3/2}$ was shifted to lower binding energy at 853.2 eV. In the Ni $2p_{3/2}$ region, the spectra have been fitted by three deconvoluted peaks at 852.3, 853.4 and 855.1 eV, which can be assigned to metallic Ni, NiO (Ni^{2+}) and Ni_2O_3 (Ni^{3+}) species, respectively. Based on the deconvoluted peaks, the relative concentration of Ni^{2+} species in the Ni–Co/MSN increased with the decrease in the Ni^{3+} species and the changes in Ni–Co/MSN is higher compared to Ni/MSN.

The Co 2p spectra of Co/MSN and Ni–Co/MSN exhibited Co $2p_{3/2}$ and Co $2p_{1/2}$ peaks at 779.1 and 793.6 eV, respectively. Deconvolution of the Co $2p_{3/2}$ peaks of both catalysts revealed the presence of metallic Co, CoO (Co^{2+}) and Co_3O_4 (Co^{3+}) at 778.2, 779.1 and 781.2 eV, respectively [24]. The binding energy of Co $2p_{3/2}$ in the Co/MSN was shifted from 779.1 eV to 781.3 eV in the Ni–Co/MSN, suggesting the domination of Co^{3+} in the latter catalyst.

The increase in the binding energy suggested the withdrawal of valence electron charge occurred through oxidation, resulting in higher oxidation state and vice versa. This result implied a *d*-electron transfer between Ni and Co in the Ni–Co/MSN, which resulted in the enrichment of electron on elemental Ni [25]. This result is in accordance with the XRD result, where an additional peak of $NiCo_2O_4$ was detected in the Ni–Co/MSN. Since the characteristic peaks of pure metal oxides were still present, only partial transformation of NiO and Co_3O_4 into Ni–Co alloy occurred.

3.1.6. Catalytic testing

The activity and stability results of Co/MSN, Ni/MSN and Ni–Co/MSN are shown in Fig. 7. Under the reaction conditions studied, Ni–Co/MSN exhibited a higher CH_4 conversion than that of Ni/MSN and Co/MSN. Previous study showed that Co-based catalyst has a lower intrinsic activity than Ni-based catalyst [19]. However, it is noteworthy that the addition of Co as a binder improved the catalytic performance of the Ni/MSN. It is widely accepted that the CO_2 reforming of CH_4 mechanism initiates with methane decomposition to produce CH_x fragments (with *x* between 0 and 3) on the catalyst's active sites [26], being this reaction as the rate limiting step of the overall process. Since CH_4 decomposition is a structure-sensitivity reaction, the particle size of the metal has been considered as the key factor to enhance the activity [27]. From the XRD and TEM analyses, it evidenced that the Ni particle size in Ni–Co/MSN was slightly reduced and the Ni dispersion was improved with respect to the Co/MSN. In fact, the small metal particle and better metal dispersion will contribute to more edges and more metal-support structures, and leading to more active sites. Furthermore, the Ni–Co alloy sites in the Ni–Co/MSN appeared to be responsible for a higher CH_4 conversion compared to the metallic Ni and Co sites in the Ni/MSN and Co/MSN, respectively. Previous studies reported that Ni and Co sites in the Ni–Co alloy are more readily accessible than those in bulk structures [1].

The importance of Ni–Co alloy formation in CO_2 reforming of CH_4 was also highlighted in the previous reports. The Ni–Co spinel is favorably formed when a sample containing Ni and Co was calcined at high temperature (>400 °C) [18]. Fakeeha et al. [28]

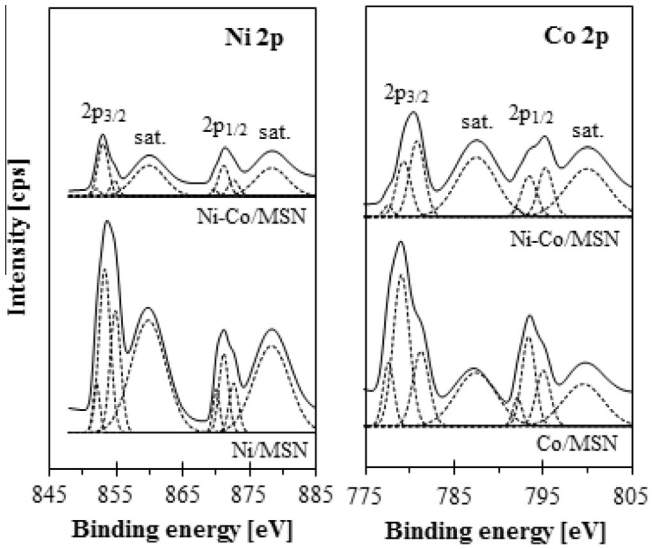

Fig. 6. XPS spectra of Ni 2p and Co 2p of Ni/MSN, Co/MSN and Ni–Co/MSN.

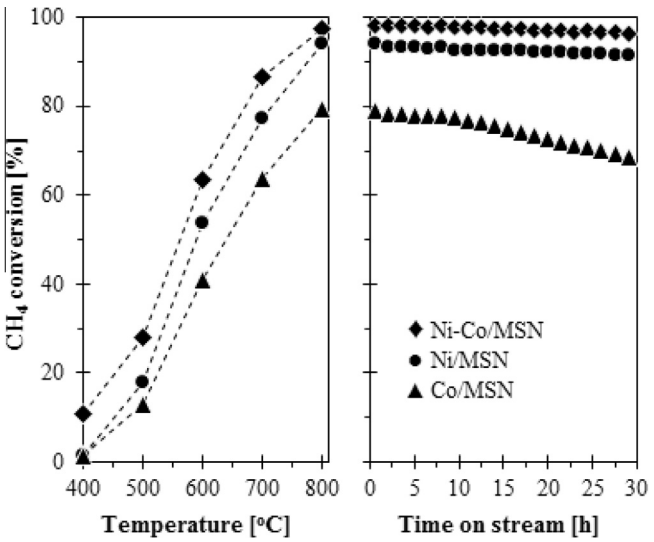

Fig. 7. Catalytic activity and stability of the Co/MSN, Ni/MSN and Ni–Co/MSN.

suggested that the formation of spinel species during the course of calcination has taken place as follows:

$$NiO + 2CoO + 0.5O_2 \rightarrow NiCo_2O_4 \quad (5)$$

However, it can be seen that the effect of Ni–Co alloy formation towards catalytic performance is greatly influenced by the operating parameters. In order to understand the effect of calcination temperature towards Ni–Co/CeO_2, the catalyst was calcined at different temperature [18]. They reported that conversion of CH_4 and CO_2 decreased with the increased of calcination temperature from 700 and 900 °C. The formation of Ni–Co spinel is less at lower calcination temperature and it increases at higher calcination temperature with increasing particle size. In another study, Xu et al. [29] concluded that the catalytic activity of the bimetallic Ni/Co catalysts supported on commercial-Al_2O_3 doped with La_2O_3 is closely related to the Ni/Co ratio. The catalyst having Ni/Co ratio of 7/3 at the total metal loading of 10 wt.% exhibited the highest CH_4 and CO_2 conversions, while further increasing the amount of Co decreased the catalytic activity. This result is in accordance with the finding reported by Zhao et al. [30], which found that increasing the Co content lead to a higher intensity of diffraction peak related to the spinel phase, indicating an increased in degree of spinel crystallization and particle size. In contrast, Estephane et al. [31] reported that the bimetallic catalyst with higher Co content (1Ni2Co/ZSM5) had a higher activity in CO_2 reforming of CH_4 compared to lower (2Ni1Co/ZSM5) or balance (1Ni1Co/ZSM5) Co/Ni ratio at the similar metal loading of 7 wt.%. Therefore, it is believed that the optimum Ni/Co ratio for a bimetallic system is varied for a catalyst depending on the effect of other operating parameters such as calcination temperature and total metal loading.

The Ni/MSN and Ni–Co/MSN showed a stable CH_4 conversion in 30 h time on stream at 800 °C. Eventhough both catalysts showed stable activity, TGA analyses for spent catalysts indicated that carbon content detected for Ni/MSN was 23% higher than Ni–Co/MSN. This may due to the incorporation of Ni in the Ni–Co solid solution, which is beneficial in preventing the generation of carbon on the Ni surface. The occurrence of electron transfer from Co to Ni during the alloying process led to the enrichment of the electron density in Ni surface and also oxygen vacancy on the Co surface [32]. This phenomenon promoted a higher CO_2 adsorption and facilitated a greater CO_2 activation, which resulted in the enhancement of carbon elimination by the reaction of oxygen with carbon intermediate to yield CO [33]. Thus, a lower coke deposit was formed on the catalyst surface and the stability of the catalyst was increased.

In addition, the mutual interaction between Ni and Co which resulted from the formation of $NiCo_2O_4$ also enhanced the stability of Ni particle. The particle size of Ni in the Ni/MSN increased about 4.2 fold from 5.62 to 23.4 nm after the stability test. Whereas the Ni–Co/MSN showed better anti-sintering ability, since the Ni particle size only increased from 3.87 to 12.8 nm (which does not exceed more than 3.3 fold form the fresh catalyst). The H_2-TPR results indicated that this species was reduced at a higher temperature as compared to the Ni/MSN. Theoretically, the stronger interaction between Ni and Co in the Ni–Co alloy, lessen the tendency of sintering during the reaction to occur [18,22]. Therefore, it could be suggested that the formation of Ni–Co alloy strengthen the interaction between the Ni and Co and increased the anti-sintering ability of the Ni particles.

As reported by the previous study, the Co-based catalyst is prone to metal deactivation by oxidation [22]. However, in this case, the incorporation of Co as the binder in the Ni–Co/MSN had boosted the activity for a longer period. From the characterization and catalytic activity results, it can be inferred that synergism occurred between Ni and Co, where these elements have a mutual role to improve the CO_2 reforming of CH_4 activity. The presence of Co as the binder significantly reduced the sintering effect and coke formation of the catalyst. Therefore, in the next section, the effect of process variables on Ni–Co/MSN in the CO_2 reforming of CH_4 was studied using DOE. A combination of statistical and mathematical techniques applied in RSM was used to obtain the optimum value of the process variables.

3.2. Optimization by RSM

The CCD was used to develop the correlation between the process variables, including reaction temperature, CO_2 to CH_4 ratio and GHSV (coded as A, B, and C, respectively) to the response, CH_4 conversion. The quadratic model for CH_4 conversion in terms of coded factors is presented in Eq. (6).

$$\begin{aligned} CH_4 \text{ conversion } [\%] = {} & 82.42 + 7.912A + 6.16B - 2.65C \\ & - 14.1AB - 2.35AC - 0.83BC \\ & - 3.67A^2 - 6.09B^2 - 8.04C^2 \end{aligned} \quad (6)$$

Table 1 shows the ANOVA for 2^3 full CCD for CH_4 conversion. Based on 90% confidence level, the model was tested to be significant as the computed F value (3.06) was higher than the theoretical $F_{0.1,9,6}$ value (2.96). This result gave an indication that the model was adequate for predicting the conversion of CH_4 within the range of variables studied. The positive sign in front of the model terms indicates synergistic effect while the negative sign shows antagonistic effect [34]. In order to determine the significant terms in the model for further analysis, the value of calculated probability (p-value) must be less than 0.100. In this study, A, AB, and C^2 were significant model terms while B, C, B^2, A^2, AC, and BC were found to be insignificant to CH_4 conversion. However, the insignificant terms were not eliminated in the model Eq. (4) in order to obtain a hierarchy model. Based on the ANOVA analysis for single variable, the most prominent significant single term that affected the conversion of CH_4 was reaction temperature (A) as indicated by the relatively large value of F-test value (5.65). An added advantage of using the DOE approach is that the interaction between process variables could be studied systematically and efficiently [17,35]. Hence, based on the data shown in Table 1, the interaction of temperature and CO_2/CH_4 ratio and quadratic interaction of GHSV were found to significantly affect the conversion of CH_4.

Fig. 8 shows the t-distribution values in a Pareto chart and the corresponding p-values of the variables in Eq. (4). The p-value serves as a tool to check the significance of each coefficient. The corresponding coefficient with a smaller p-value or a t-value with a greater magnitude donates more significance into the model. For a model to be reliable, the response should be predicted with an acceptable accuracy and compared with the experimental data. Through the ANOVA analysis, it was found that the value of correlation coefficient, R^2 was 0.8439. According to Haaland, the empirical model is adequate to explain most of the variability in the essay reading, which should be at least 0.75 or greater [36]. Response surfaces and contour plots are generally used to evaluate relationships between the variables and to predict the results under given conditions. The plots of the response surface and contour of CH_4 conversion were drawn as a function of two significant factors at a time, holding all other factors at the zero level using Eq. (6) and are presented in Fig. 9. The interactions between the corresponding variables were insignificant when the contour of the response was circular [15]. On the contrary, interactions between the relevant variables were significant when the contour of the response surfaces was elliptical. Notably, all contour plots in Fig. 9 were elliptical, indicating significant interaction effects between the variables studied.

Fig. 9A illustrates CO_2:CH_4 ratio and GHSV effects on CH_4 conversion. The CH_4 conversion showed a volcano-shaped trend with respect to the GHSV. An increase in the GHSV increased the CH_4

Table 1
Analysis of variance (ANOVA) for 2^3 center composite design (CCD) for CH_4 conversion.

Response	Factor	Sum of squares	Degree of freedom	Mean square	*F*-test	*p*-value
CH_4 conversion [%]	Model	4175	9	463.97	3.06	
	A	855.78	1	855.78	5.650	0.054
	B	124.78	1	124.78	0.824	0.399
	C	517.15	1	517.15	3.418	0.114
	A^2	343.80	1	343.80	2.272	0.182
	B^2	95.79	1	95.79	0.633	0.457
	C^2	598.31	1	598.31	3.954	0.094
	AB	1590.48	1	1590.48	10.51	0.018
	AC	44.18	1	44.18	0.292	0.608
	BC	5.45	1	5.45	0.036	0.856
	Error	907.81	6	151.30		
	Total SS	5082.81	15			

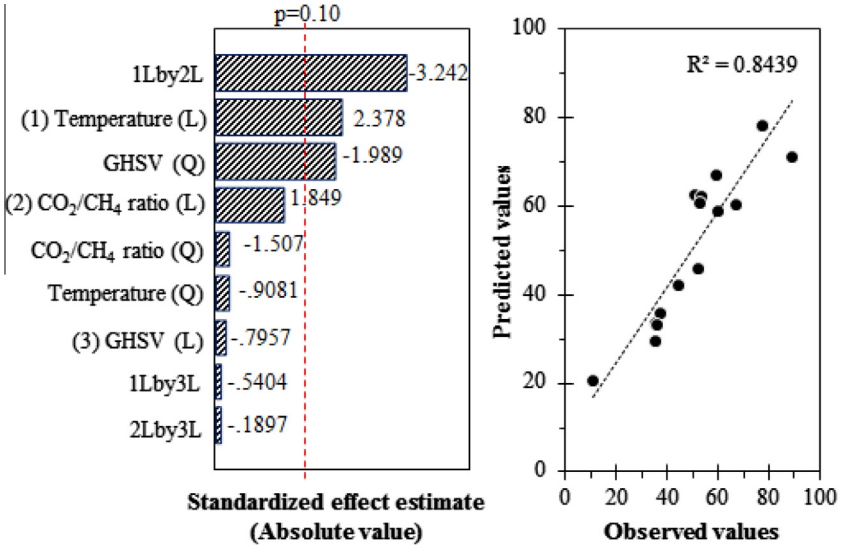

Fig. 8. (A) Pareto chart and (B) predicted vs observed value plot of the model.

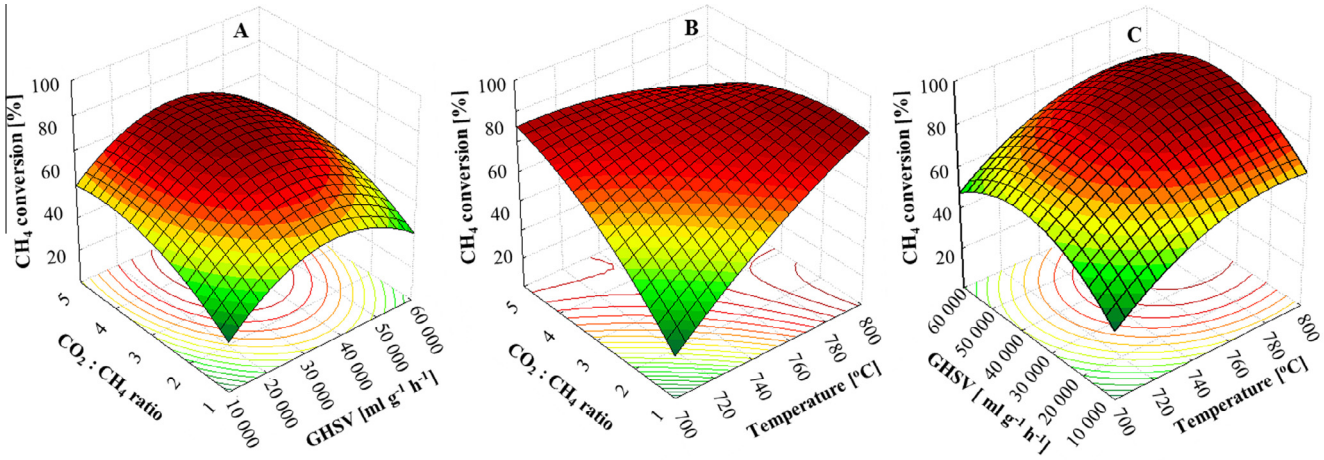

Fig. 9. Response surface plot of the combined (A) CO_2:CH_4 ratio and GHSV, (B) CO_2:CH_4 ratio and reaction temperature, and (C) GHSV and reaction temperature.

conversion. Once the CH_4 conversion reached its highest level, a further increase in the value of the GHSV decreased the CH_4 conversion. The effect of GHSV or residence time in the present study was similar to the result reported in the literature which indicated that the increase in GHSV value decreased the conversion of CH_4. This may be due to the shorter contact time for the reactants to interact with the catalyst, thus reducing its catalytic activity [37].

A similar effect of CO_2:CH_4 ratio was also observed in Fig. 9B, which demonstrated the effect of CO_2:CH_4 ratio and reaction temperature on CH_4 conversion. The CH_4 conversion increased gradually with the increasing of CO_2:CH_4 ratio from 1 to 5. This observation indicated that the CO_2 can acts as an active oxidant and has a positive effect on the CH_4 conversion [38]. This result could be explained through the disproportionation reaction by

the Le Chatelier's principal which expected that the surpass CO_2 could enhance the amount of CH_4 being converted to CO and H_2, thus resulting in the increase of CH_4 conversion [39].

From the analysis of the response surface plot, the reaction temperature exhibited the most significant influence on the response surface in comparison to the GHSV and CO_2:CH_4 ratio, as could be seen in Fig. 9B and C, respectively. This can be explained by a larger t-value for the reaction temperature as compared to the other variables. The CH_4 conversion was considerably improved at higher reaction temperature due to the endothermic nature of the CO_2 reforming of CH_4 reaction [40]. The optimum CH_4 conversion predicted form the response surface analysis is 97% at reaction temperature of 783 °C, CO_2:CH_4 ratio of 3, and GHSV of 38,726 mL g_{cat}^{-1} h^{-1}. An additional experiment was carried out to validate the optimization results obtained by response surface analysis. The CH_4 conversion of experiment at optimum conditions is 96.3% and the difference between the predicted and observed values is 0.7%.

4. Conclusions

In this study, Ni–Co/MSN was successfully prepared by consecutive in situ electrolysis. XRD and TEM analyses demonstrated that the Ni–Co/MSN has smaller and better dispersion of metal particles with respect to the Ni/MSN and Co/MSN. The addition of Co as the binder in Ni–Co/MSN favored the formation of $NiCo_2O_4$ solid solution, as proven by XRD and XPS analyses. H_2-TPR results indicated that the formation of Ni–Co alloy increased the reduction temperature, suggesting stronger interaction between Ni and Co in the catalyst. The Ni–Co/MSN catalyst demonstrated excellent performance for CO_2 reforming of CH_4. The synergy effect between Ni and Co in the $NiCo_2O_4$ not only provided high activity, but also a better carbon tolerant and anti-metal sintering ability, with a stable performance for more than 30 h time on stream. The interaction between process variables was studied using CCD by applying 2^3 factorial points with one response parameter (CH_4 conversion). The Pareto chart and ANOVA analysis indicated that the reaction temperature was the most important single variable in CO_2 reforming of CH_4. The optimum CH_4 conversion predicted from the response surface analysis is 97% at an operating reaction temperature of 783 °C, CO_2:CH_4 ratio of 3, and GHSV of 38,726 mL g^{-1} h^{-1}.

Acknowledgement

This work is supported by the Universiti Teknologi Malaysia through Research University Grant No. 05H09. Our gratitude also goes to the Ministry of Higher Education (MOHE) Malaysia for the award of MyPhD Scholarship (Siti Munirah Sidik) and the Hitachi Scholarship Foundation for the Gas Chromatograph Instrument Grant.

Appendix A. Supplementary data

Supplementary data associated with this article can be found, in the online version, at http://dx.doi.org/10.1016/j.cej.2016.03.041.

References

[1] J. Zhang, H. Wang, A.K. Dalai, Development of stable bimetallic catalysts for carbon dioxide reforming of methane, J. Catal. 249 (2007) 300–310.
[2] Y. Kathiraser, U. Oemer, E.T. Saw, Z. Li, S. Kawi, Kinetic and mechanistic aspects for CO_2 reforming of methane over Ni based catalysts, Chem. Eng. J. 278 (2015) 62–78.
[3] A.A. Ibrahim, A.H. Fakeeha, A.S. Al-Fatesh, Enhancing hydrogen production by dry reforming process with strontium promoter, Int. J. Hydrogen Energy 39 (2014) 1680–1687.
[4] D. Liu, X.Y. Quek, W.N.E. Cheo, R. Lau, A. Borgna, Y. Yang, MCM-41 supported nickel-based catalysts with superior stability during carbon dioxide reforming of methane: effect of strong metal-support interaction, J. Catal. 266 (2009) 380–390.
[5] S.R. Yahyavi, M. Haghighi, S. Shafiei, M. Abdollahifar, F. Rahmani, Ultrasound-assisted synthesis and physicochemical characterization of Ni–Co/Al_2O_3-MgO nanocatalysts enhanced by different amounts of MgO used for CH_4/CO_2 reforming, Energy Convers. Manage. 97 (2015) 273–281.
[6] M.-S. Fan, A.Z. Abdullah, S. Bhatia, Utilization of greenhouse gases through carbon dioxide reforming of methane over Ni–Co/MgO–ZrO_2: preparation, characterization and activity studies, Appl. Catal. B: Environ. 100 (2010) 365–377.
[7] A.H. Karim, A.A. Jalil, S. Triwahyono, S.M. Sidik, N.H.N. Kamarudin, R. Jusoh, N. W.C. Jusoh, B.H. Hameed, Amino modified mesostructured silica nanoparticles for efficient adsorption of methylene blue, J. Colloid Inter. Sci. 386 (2012) 307–314.
[8] N.H.N. Kamarudin, A.A. Jalil, S. Triwahyono, N.F.M. Salleh, A.H. Karim, R.R. Mukti, B.H. Hameed, R. Ahmad, Role of 3-aminopropyltriethoxysilane in the preparation of mesoporous silica nanoparticles for ibuprofen delivery: effect on physicochemical properties, Microporous and Mesoporous Mater. 180 (2013) 235–241.
[9] M.A.A. Aziz, A.A. Jalil, S. Triwahyono, R.R. Mukti, Y.H. Taufiq-Yap, M.R. Sazegar, Highly active Ni-promoted mesostructured silica nanoparticles for CO_2 methanation, Appl. Catal. B: Environ. 147 (2014) 359–368.
[10] S.M. Sidik, A.A. Jalil, S. Triwahyono, T.A.T. Abdullah, A. Ripin, CO_2 reforming of CH_4 over Ni/mesostructured silica nanoparticles (Ni/MSN), RSC Adv. 5 (2015) 37405–37414.
[11] S.M. Sidik, S. Triwahyono, A.A. Jalil, M.A.A. Aziz, N.A.A. Fatah, L.P. Teh, Tailoring the properties of electrolyzed Ni/mesostructured silica nanoparticles (MSN) via different Ni-loading methods for CO_2 reforming of CH_4, J. CO_2 Util. 13 (2016) 71–80.
[12] A.A. Jalil, N. Kurono, M. Tokuda, Facile synthesis of Ethyl 2-Arylpropenoates by Cross-coupling reaction using electrogenerated highly reactive zinc, Tetrahedron 58 (2002) 7477–7484.
[13] M.A. Bezerra, R.E. Santelli, E.P. Oliveira, L.S. Villar, L.A. Escaleira, Response surface methodology (RSM) as a tool for optimization in analytical chemistry, Talanta 76 (2008) 965–977.
[14] M.V. Gil, J. Fermoso, F. Rubiera, D. Chen, H_2 production by sorption enhanced steam reforming of biomass-derived bio-oil in a fluidized bed reactor: an assessment of the effect of operation variables using response surface methodology, Catal. Today 242 (2015) 19–34.
[15] M.-S. Fan, A.Z. Abdullah, S. Bhatia, Hydrogen production from carbon dioxide reforming of methane over Ni–Co/MgO-ZrO_2 catalyst: process optimization, Inter. J. Hydrogen Energy 36 (2011) 4875–4886.
[16] M. Usman, W.W. Daud, H.F. Abbas, Dry reforming of methane: influence of process parameters—a review, Renew. Sust. Energy Rev. 45 (2015) 710–744.
[17] M.A.A. Aziz, A.A. Jalil, S. Triwahyono, M.W.A. Saad, CO_2 methanation over Ni-promoted mesostructured silica nanoparticles: influence of Ni loading and water vapor on activity and response surface methodology studies, Chem. Eng. J. 260 (2015) 757–764.
[18] H. Ay, D. Üner, Dry reforming of methane over CeO_2 supported Ni, Co and Ni–Co catalysts, Appl. Catal. B: Environ. 179 (2015) 128–138.
[19] S. Sengupta, G. Deo, Modifying alumina with CaO or MgO in supported Ni and Ni–Co catalysts and its effect on dry reforming of CH_4, J. CO_2 Util. 10 (2015) 67–77.
[20] N.W.C. Jusoh, A.A. Jalil, S. Triwahyono, C.R. Mamat, Tailoring the metal introduction sequence onto mesostructured silica nanoparticles framework: effect on physicochemical properties and photoactivity, Appl. Catal. A: Gen. 492 (2015) 169–176.
[21] V.G. Deshmane, S.L. Owen, R.Y. Abrokwah, D. Kuila, Mesoporous nanocrystalline TiO2 supported metal (Cu Co, Ni, Pd, Zn and Sn) catalysts: effect of metal-support interactions on steam reforming of methanol, J. Mol. Catal. A: Chem. 408 (2015) 202–213.
[22] I.G.O. Črnivec, P. Djinović, B. Erjavec, A. Pintar, Effect of synthesis parameters on morphology and activity of bimetallic catalysts in CO_2-CH_4 reforming, Chem. Eng. J. 207 (2012) 299–307.
[23] W. Zhen, B. Li, G. Lu, J. Ma, Enhancing catalytic activity and stability for CO_2 methanation on Ni–Ru/γ-Al_2O_3 via modulating impregnation sequence and controlling surface active species, RSC Adv. 4 (2014) 16472–16479.
[24] K. Takanabe, K. Nagaoka, K. Nariai, K. Aika, Titania-supported cobalt and nickel bimetallic catalysts for carbon dioxide reforming of methane, J. Catal. 232 (2005) 268–275.
[25] Y. Yu, Q. Jin, Y. Wang, X. Guo, Synthesis of natural gas from CO methanation over SiC supported Ni–Co bimetallic catalysts, Catal. Commun. 31 (2013) 5–10.
[26] D. Pakhare, V. Schwartz, V. Abdelsayed, D. Haynes, D. Shekhawat, J. Poston, J. Spivey, Kinetic and mechanistic study of dry (CO_2) reforming of methane over Rh-substituted $La_2Zr_2O_7$ pyrochlores, J. Catal. 316 (2014) 78–92.
[27] M. Garcia-Dieguez, E. Finocchio, M.A. Larrubia, L.J. Alemany, G. Busca, Characterization of alumina-supported Pt, Ni, and PtNi alloy catalysts for the dry reforming of methane, J. Catal. 274 (2010) 11–20.
[28] A.H. Fakeeha, W.U. Khan, A.S. Al-Fatesh, A.E. Abasaeed, M.A. Naeem, Production of hydrogen and carbon nanofibers from methane over Ni–Co-Al catalysts, Inter. J. Hydrogen Energy 40 (2015) 1774–1781.
[29] J. Xu, W. Zhou, Z. Li, J. Wang, J. Ma, Biogas reforming for hydrogen production over nickel and cobalt bimetallic catalysts, Inter. J. Hydrogen Energy 34 (2009) 6646–6654.

[30] M. Zhao, T.L. Church, A.T. Harris, SBA-15 supported Ni–Co bimetallic catalysts for enhanced hydrogen production during cellulose decomposition, Appl. Catal. B: Environ. 101 (2011) 522–530.
[31] J. Estephane, S. Aouad, S. Hany, B.E. Khoury, C. Gennequin, H.E. Zakhem, J.E. Nakat, A. Aboukaïs, E.A. Aad, CO2 reforming of methane over Ni–Co/ZSM5 catalysts. Aging and carbon deposition study, Inter. J. Hydrogen Energy 40 (2015) 9201–9208.
[32] R. Wang, H. Xu, X. Liu, Q. Ge, W. Li, Role of redox couples of $Rh^0/Rh^{\delta+}$ and Ce^{4+}/Ce^{3+} in CH_4/CO_2 reforming over Rh-CeO_2/Al_2O_3 catalyst, Appl. Catal. A: Gen. 24 (2006) 204–210.
[33] C. Li, P.J. Tan, X.D. Li, Y.L. Du, Z.H. Gao, W. Huang, Effect of the addition of Ce and Zr on the structure and performances of Ni–Mo/CeZr–MgAl(O) catalysts for CH_4-CO_2 reforming, Fuel Process. Technol. 140 (2015) 39–45.
[34] Z.Y. Zakaria, N.A.S. Amin, J. Linnekoski, Optimization of catalytic glycerol steam reforming to light olefins using Cu/ZSM-5 catalyst, Energy Convers. Manage. 86 (2014) 735–744.
[35] H.D. Setiabudi, A.A. Jalil, S. Triwahyono, N.H.N. Kamarudin, R. Jusoh, Ir/Pt-HZSM-5 for *n*-pentane isomerization. Effect of Si/Al ratio and reaction optimization by response surface methodology, Chem. Eng. J. 217 (2013) 300–309.
[36] P.D. Haaland, Experimental Design in Biotechnology, Marcel Dekker Inc., New York, 1989.
[37] N. Rahemi, M. Haghighi, A.A. Babaluo, S. Allahyari, M.F. Jafari, Syngas production from reforming of greenhouse gases CH_4/CO_2 over Ni–Cu/Al_2O_3 nanocatalyst: impregnated vs plasma-treated catalyst, Energy Convers. Manage. 84 (2014) 50–59.
[38] F. Mirzaei, M. Rezaei, F. Meshkani, Z. Fattah, Carbon dioxide reforming of methane for syngas production over Co-MgO mixed oxide nanocatalysts, J. Ind. Eng. Chem. 21 (2015) 662–667.
[39] M. Khavarian, S.-P. Chai, A.R. Mahamed, The effects of process parameter on carbon dioxide reforming of methane over Co-Mo-MgO/MWCNTs nanocomposite catalysts, Fuel 158 (2015) 129–138.
[40] Y. Vafaeian, M. Haghighi, S. Aghamohammadi, Ultrasound assisted dispersion of different amount of Ni over ZSM-5 used as nanostructured catalyst for hydrogen production via CO_2 reforming of methane, Energy Convers. Manage. 76 (2013) 1093–1103.